A radar backscatter simulation of a forest canopy using 3D physical structures derived from LiDAR scanning

Article

Published Version

Creative Commons: Attribution 4.0 (CC-BY)

Open Access

Escobar Ruiz, V. ORCID: https://orcid.org/0000-0003-1336-0921, Maslanka, W., Westbrook, C. ORCID: https://orcid.org/0000-0002-2889-8815, Morrison, K. ORCID: https://orcid.org/0000-0002-8075-0316, Calders, K., Origo, N., Disney, M. and Fox, N. (2024) A radar backscatter simulation of a forest canopy using 3D physical structures derived from LiDAR scanning. International Journal of Remote Sensing. ISSN 1366-5901 doi: https://doi.org/10.1080/01431161.2024.2403626 Available at https://centaur.reading.ac.uk/118919/

It is advisable to refer to the publisher's version if you intend to cite from the work. See Guidance on citing.
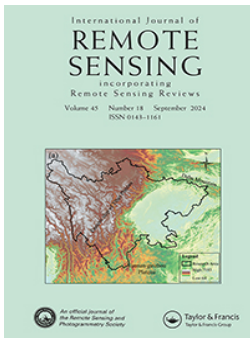
To link to this article DOI: http://dx.doi.org/10.1080/01431161.2024.2403626

Publisher: Taylor & Francis

CentAUR

Central Archive at the University of Reading

Reading's research outputs online

A radar backscatter simulation of a forest canopy using 3D physical structures derived from LiDAR scanning

Veronica Escobar-Ruiz, William Maslanka, Chris D. Westbrook, Keith Morrison, Kim Calders, Niall Origo, Mathias Disney & Nigel Fox

View supplementary material ⧉

Published online: 08 Oct 2024.

Submit your article to this journal ⧉

View related articles ⧉

View Crossmark data ⧉

Taylor & Francis
Taylor & Francis Group

A radar backscatter simulation of a forest canopy using 3D physical structures derived from LiDAR scanning

Veronica Escobar-Ruiz [ID][a], William Maslanka[b], Chris D. Westbrook[a], Keith Morrison [ID][a], Kim Calders[c], Niall Origo[d], Mathias Disney[e,f] and Nigel Fox[d]

[a]Meteorology Department, University of Reading, Reading, UK; [b]Geography Department, King's College London, London, UK; [c]Q-ForestLab, Department of Environment, Faculty of Bioscience Engineering, Ghent University, Ghent, Belgium; [d]Earth Observation, Climate and Earth Observation group - National Physical Laboratory, Teddington, UK; [e]Department of Geography, University College London, London, UK; [f]NERC National Centre for Earth Observation (NCEO), University College London, London, UK

ABSTRACT

This study aims to explore the forest aboveground biomass relationship to C-band backscatter. A one-hectare area in Wytham Woods, located west of Oxford, was selected for this research. The area has a total of 525 trees of seven different tree species. The Michigan Microwave Canopy Scattering Model (MIMICS), a two-layer radiative transfer model, was applied to simulate canopy backscatter responses in this deciduous UK forest. Model parameters related to forest structure were derived from previously published terrestrial laser (LiDAR) data. Simulated backscatter was performed for co-polarized and cross-polarized modes at a C-band frequency range and incidence angles (20° to 45° at 5° increments). The research includes five objectives: i) backscatter sensitivity analysis from the variation of different model parameters; ii) backscatter seasonal effect under spring–summer (leaf-on) and autumn–winter (leaf-off) periods; iii) backscatter comparison between species as well as between simulated and satellite observations in a spatial pattern; iv) relationship between simulated backscatter and aboveground biomass; and v) relationship between MIMICS forest structure parameters and simulated backscatter. Sensitivity analysis results showed significant differences in backscatter from changes in leaf distribution, leaf thickness and water content (leaf, trunk and soil) for both polarization modes in leaf-on scenarios. Leaf-off scenarios presented significant differences from changes in branch distribution but only for the co-polarized mode. Seasonal variations presented significant backscatter differences between spring–summer and autumn–winter scenarios; additionally, backscatter differences among species for each seasonality in the co-polarized mode were observed. The computation of the grid resolution (20 m × 20 m) showed a range of backscatter values depending on the grid and incidence angle. Higher backscatter values were observed for the satellite data than for the simulated data. Finally,

CONTACT Veronica Escobar-Ruiz ✉ v.escobarruiz@reading.ac.uk ▣ Meteorology Department, University of Reading, Brian Hoskins Building, Reading 1U06, UK

the aboveground biomass and the MIMICS input parameters presented high random variability and little systematic co-variation with the total backscatter on both simulated seasons, suggesting that more robust allometric equations for biomass estimation are required.

1. Introduction

Forest areas are large sinks of atmospheric carbon dioxide at ground level, via absorption into the plant tissue through photosynthesis, and account for almost 72% of terrestrial carbon in woody biomass and soil (Malhi, Meir, and Brown 2002). Nonetheless, for some forests, the carbon sink is drastically declining (Hubau et al. 2020). This means that knowledge of the amount of biomass is essential for an understanding of the current state of the climate and parameterization in future climate change modelling. Understanding the aboveground biomass (AGB), the 'aboveground standing dry mass of live or dead matter from tree or shrub (woody) life forms expressed as a mass per unit area' (Wilkes et al. 2018), is so important that it has been designated an Essential Climate Variable (ECV) in the Global Climate Observation System (GCOS).

Optical satellite observations have been commonly used to estimate AGB for forested areas, for example, the Normalized Difference Vegetation Index (NDVI, Raymond and Chaturvedi 2020; Zhu and Liu 2015) and the Bidirectional Reflectance Distribution Function (BRDF, Kumar and Mutanga 2017; Pisek et al. 2021), with the latter used to obtain forest physical parameters that are subsequently used for forest carbon modelling. Similarly, LiDAR instruments in satellites have been applied for AGB estimation. However, the frequency used to emit the laser pulse is unable to penetrate clouds, hence, to get a cloud-free mosaic for an accurate AGB, the satellite requires multiple-day composites. The lack of continuous data contributes to high uncertainty in AGB prediction (Lu et al. 2012). On this basis, radar satellite observations have some advantages over optical observations due to their cloud-penetrating properties. Furthermore, radar data can be used in conjunction with optical observations for forest characterization and biomass mapping purposes (Badreldin and Sanchez-Azofeifa 2015). Space-based radar remote sensing observations have been widely used to estimate AGB using Synthetic Aperture Radar (SAR, de Jesus et al. 2023; Wang et al. 2024; Zeng et al. 2022) and Interferometric SAR (InSAR, Balzter, Rowland, and Saich 2007). However, the resolution of the radar data (for example, approximately 20 m × 20 m for Sentinel-1, Maslanka et al. 2022)means that multiple trees are often present in a single pixel, and thus validation via field measurements is often required (Liu et al. 2015), with data aggregation and upscaling to pixel scale often being considered (Zhen et al. 2022).

Relationships between polarimetric SAR backscatter (C- and L-bands) and forest biomass have previously been obtained (Zeng et al. 2022). However, the SAR backscatter intensity is strongly dependent on tree species (Imhoff 1995). This variation in backscatter intensity with respect to tree species within a pixel has led to differences in estimated AGB, observed by space-based remote sensing techniques (Mitchard et al. 2012).

Additionally, AGB can be estimated using empirical allometric models (Bunce 1968; Chung et al. 2017; Kim et al. 2022); these models describe the relationship between

measurable ecological variables, typically using either tree height or trunk diameter, or both. However, errors in AGB predictions related to empirical model uncertainty (Kim et al. 2022) can contribute to significant discrepancies between climatic models (Rollinson et al. 2017). These ecological variables can be obtained with *in-situ* field measurements using either destructive (direct) or non-destructive (indirect) methods. Examples of destructive methods include harvesting and weighing plant samples from a study area (Calders et al. 2014; Lu et al. 2014), while non-destructive field measurements include ground-based remote sensing techniques such as Terrestrial Laser Scanning (TLS), also known as terrestrial LiDAR (Calders et al. 2014; de Tanago et al. 2017; Takoudjou et al. 2017).

Whilst field measurements can accurately estimate AGB for a forested region, the collection of field observations is time-consuming and geographically limited to specific regions of study. Therefore, space-based remote sensing has been mostly used to globally estimate AGB using backscatter intensity (Englhart, Keuck, and Siegert 2011; Saatchi et al. 2007). Furthermore, due to the disadvantages of Lidar technology in satellite systems (e.g. sensitivity to clouds and atmospheric particles), satellite-radar data has become more popular; making use of the repeating orbits of satellites to cover the globe and observe regions that are more difficult to reach in person. Nonetheless, it is extremely difficult and complex to quantify the individual contributions of vegetation parameters to the radar backscatter signal. Hence, where forested areas can be parameterized and the radar backscatter can be simulated, modelling approaches are often used to understand the microwave scattering properties of the forest canopy (Le Toan et al. 1992), which in turn is crucial for interpreting remote sensing data accurately (Treuhaft and Siqueira 2004). Furthermore, simulating radar responses over time can help understand how changes in biomass, such as growth, deforestation and forest degradation, affect satellite radar signals (Hethcoat et al. 2021).

Under the radiative transfer (RT) theory (Tsang, Kong, and Shin 1984), several models have been developed for the simulation of electromagnetic scattering in forest areas (Karam and Fung 1988; Lang and Sighu 1983). Other scattering approaches include the distorted Bron approximation based on Maxwell's equation (Yi-Cheng and Sarabandi 1995). In RT theory, a two-layer model consists of endless horizontal layers, the top one representing the canopy (branches and leaves), a mid-layer consisting of trunks, and a bottom layer simulating the ground. Foliage at the upper layer is characterized as randomly oriented non-spherical objects and the ground is modelled as a rough surface. Other approaches include the treatment of each tree as an individual backscatter object (Guoqing and Jon Ranson 1995; Sun, Simonett, and Strahler 1991). In the RT theory, energy transport equations can be solved using a discrete ordinate and eigenvalue approach (Picard et al. 2004) or the Monte Carlo method (Chuah and Tan 1992; Yang et al. 2017).

Despite the diversity in backscatter simulation models, the availability of models and guidance is not always possible. Therefore, the accessibility of the Michigan Microwave Canopy Scattering Model (MIMICS) (Ulaby et al. 1990a) over other models makes it popular in the research community. Moreover, the model has been applied worldwide to simulate backscatter responses in a variety of forests (Bosisio and Dechambre 2010;

Grover, Quegan, and da Costa Freitas 1999; Karam et al. 1995; Ningthoujam et al. 2016) given a reliability on model performance.

This study aims to use the MIMICS model to assess the relationship between estimated values of AGB and the simulated C-band backscatter signal using TLS data collected in Wytham Woods, UK. The study comprises five objectives:

(1) Determine the significant changes in simulated backscatter through a sensitivity analysis of different vegetations and radiometric parameters within the MIMICS model.
(2) Examine the seasonal impacts on simulated backscatter to respectively assess spring–summer and autumn–winter periods through simulations of leaf-on and leaf-off scenarios.
(3) Calculate the mean simulated backscatter for each tree within the 1-ha study region of Wytham Woods to estimate differences between species, as well as spatial differences in backscatter patterns between simulated and contemporaneous satellite observations (Sentinel-1) in both leaf-on and leaf-off conditions with the resolution of 20 m × 20 m.
(4) Assess the relationship between simulated backscatter (VV and VH) and AGB values, derived from allometric equations.
(5) Determine the relationship between MIMICS forest structure parameters (e.g. tree height and 1st order branch density) and simulated backscatter (VV and VH) of each tree in the 1-ha.

2. Materials and methods

2.1. Materials

2.1.1. Michigan microwave canopy scattering model (MIMICS)

MIMICS (Ulaby et al. 1990a, 1990b) is a two-layer radiative transfer model that simulates canopy backscatter responses under a discrete scatterer approach. The model divides a forest vertically into three regions: a crown layer, a trunk layer, and a rough-surface ground layer. The crown layer of an individual tree is assumed to be either an oblate spheroid if the crown thickness is greater than the crown diameter or a prolate spheroid if the crown thickness is less than the crown diameter and is treated as a mixture of leaves, needles, and branches. Leaves are modelled as flat rectangular discs with dimensions a and b in the major and minor dimensions, with angle orientations characterized by a Probability Distribution Function (PDF). Branches and needles are modelled as dielectric cylinders of length L and diameter d_c, also with angle orientations characterized by a PDF. The trunk region is characterized by an average height H and an average diameter D_c. Multiple trees can be modelled by parameterizing a tree density value N, where MIMICS will assume them to be vertical cylinders randomly distributed on a horizontal plane. The rough-surface ground layer can consist of either soil, water, or snow. Soil is modelled as a dielectric material, with a roughness correlation function denoting the surface roughness. Snow can be modelled on top of the soil, with snow thickness being parameterized, whereas water is parameterized in terms of its salinity.
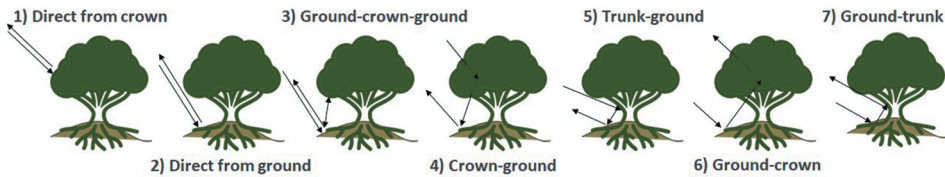
Figure 1. MIMICS backscatter components, adapted from (Ulaby et al. 1990b). 1) direct from the crown, 2) direct from ground, 3) interaction ground-crown-ground, 4) interaction crown-ground, 5) trunk-ground, 6) ground-crown and 7) ground-trunk. The sum of all components corresponds to the total backscatter.

The total backscatter is a combination of first-order scattering mechanisms, consisting of seven components (Figure 1) in which the sum of all components corresponds to the total backscatter. The model output provides the polarization modes, VV, VH, HV and HH at user-defined incidence angles and frequencies, within its operational range of 1 GHz–10 GHz. Here, only VV and VH backscatters are reported, due to the similarity in values between VV and HH (co-polarization) and VH and HV (cross-polarizations). In this contribution, MIMICS was used to retrieve the simulated backscatter signals across the C-band range, 4 GHz to 8 GHz in 2 GHz increments, with incidence angles between 20° and 45° in 5° increments. This was done to simulate the range of incidence angles experienced in a Sentinel-1 Interferometric Wide (IW) swath, 29.1° to 46.0° (Bourbigot et al. 2016)

2.1.2. Study area

Wytham Woods (51°47′N, 1°20′W) is a deciduous forest located to the west of Oxford in Southern England, UK. The mean annual rainfall (1993–2008) is 726 mm, and the mean annual radiation is 118 Wm^{-2} (Butt et al. 2009). Its mean annual 2 m air temperature (2014–2017, Cooper et al. 2021; Stanley et al. 2023) is 10.6°C, with mean daily air temperature ranging from 24.2° in the summer (JJA) and −0.6° during the winter (DJF). Similar mean annual values, in the same 3-year period, were recorded for soil temperature at 10 cm above ground and 5 cm below the surface. Additionally, volumetric water content registered a maximum of 54.9 m^3/m^3 in the winter (DJF) and a minimum of 23.1 m^3/m^3 in the summer (JJA), with a mean annual value of 42.3 m^3/m^3. Soil in the area has been classified as shallow loam over limestone (Cranfield University 2024) with a soil texture of 40% sand, 40% clay and 20% silt. For this study, trees within a 1-ha region (Figure 2) were scanned using TLS collected by Calders et al. (2018) to obtain specific parameters for the MIMICS model. This 1-ha region has previously been the focus of intensive studies (Calders et al. 2018; Kim et al. 2022; Terryn et al. 2020), which used TLS from a larger 6-ha, with the SW co-ordinates being recorded with differential GPS to be located at Lat 51.77550579, Lon −1.33904729 (Origin of Local co-ordinates, [0,0]). The 1-ha subset for this study is identical to that of the study by Calders et al. (2018), with local coordinates for the SW and NE corners being (40, 100) and (140, 200), respectively. The area of interest was dominated by Sycamore trees (*Acer pseudoplatanus*) followed by Ash (*Fraxinus excelsior*) and Hazel (*Corylus avellana*) amongst other minority species (Hawthorn [*Crataegus monogyna*], Oak [*Quercus robur*], and Maple [*Acer campestre*]). Several unidentified species of trees, categorized as 'unknown', were also present in the area.
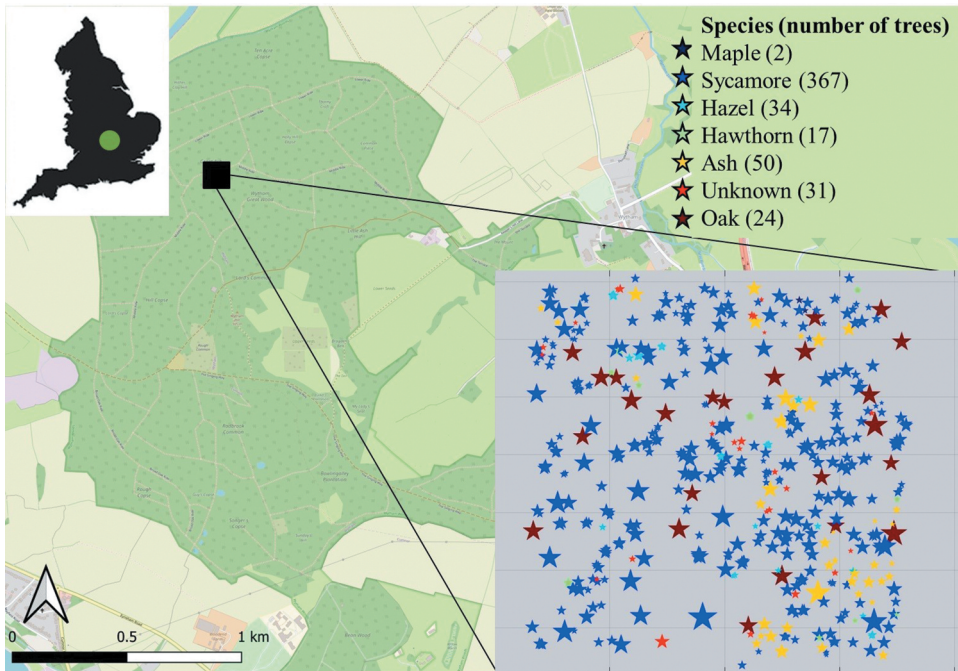
Figure 2. Location of the 1-ha area of interest (black square) inside Wytham Wood. Map data copyrighted OpenStreetMap contributors. (OpenStreetMap 2017).

2.1.3. Data collection and processing

TLS was used in conjunction with a semi-automated framework to scan, digitize, and create a virtual 3D forest, comprising the 1-ha subregion of Wytham Woods. A full description of the TLS method and workflow can be found in Calders et al. (2018). Briefly, TLS data were collected over a 6-ha region in leaf-on and leaf-off conditions. Following this, forest stand reconstruction was conducted, consisting of three main steps: tree segmentation, tree structure modelling, and leaf addition. The virtual 3D forest model consisted of leaf-on and leaf-off scans, corresponding to TLS data collected over June–July 2015 and December 2015–January 2016, respectively.

Structural variables were extracted from the 3D models that could be used to parameterize the radiative transfer model. Individual trees were defined via an identifier (a 'scene' and 'tree' number), as well as additional parameters (vertical resolution, and search radius). In summary, all object data files associated with unique identifiers are organized as a structure, containing all filenames regarding the individual tree. From this metadata structure, the points are used to determine the 3D extent of the canopy and tree. Then, the points associated with leaves are modelled as tetragons, and the associated leaf parameters are calculated (canopy thickness, canopy base height, canopy size, leaf density, and mean leaf diameter). Next, the points associated with the woody material (referred to as 'stems') are used to create a 3D geometric structure of stack cylinders, representing the woody material of the tree. Horizontal slices were taken, using the defined vertical resolution, to compute the angles between adjacent stem cylinders and thus identify and define branch hierarchy. The mean branch length and radius were calculated for all branch hierarchies. Finally, the calculated MIMICS input variables were created.
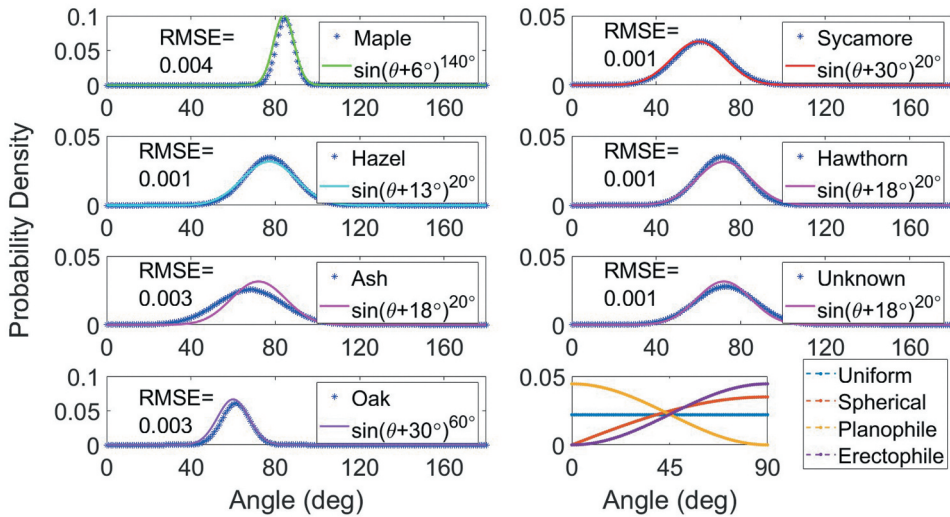
Figure 3. Measured data (dark blue dots) versus 1st and 2nd-order branches model probability distribution for each species: Maple (light green), Sycamore (red), Hael (cyan), Oak (light purple), Hawthorn, Ash and Unknown (magenta) with their corresponding calculated error (RMSE) as well as probability function of leaf angle distribution (light blue, orange, yellow and dark purple dotted lines).

To parametrize the orientation of the 1st and 2nd order branches within MIMICS, PDFs were generated from the observed orientations of the 1st and 2nd order branches of each species (Figure 3). For each species, PDFs were also modelled, to attempt to capture the distribution, with the root mean square error (RMSE) being calculated to determine the accuracy of the modelled branch distribution. Concerning the leaf angle distribution (LAD), data do not exist for the Wytham Woods species, and an assumption was made based on the author's field experience. Hence, a uniform distribution was assumed (Figure 3). For MIMICS parameters that were not possible to obtain from the TLS data or the literature, the MIMCIS default values were used (Appendix A).

Note: erectophile was not used in the simulations as Wytham Wood species do not follow this leaf distribution but was provided as a reference to see the differences between typical LADs.

2.2. Methods

2.2.1. Model sensitivity analysis

One-at-a-time (OAT) sensitivity analysis was conducted to evaluate the sensitivity of the MIMICS model to individual parameters. Parameters from a baseline simulation were incrementally changed, with the changes being based on literature values or from measured data: from TLS observations or *in-situ* field observations. The parameters chosen for the OAT sensitivity analysis were a) leaf angle distribution, b) leaf thickness, c) branch distribution, d) temperature, e) gravimetric water content (leaf, trunk and soil) and f) soil roughness (Table 1 details the range of values used for the OAT sensitivity analysis). OAT sensitivity analysis of branch distribution was also evaluated for leaf-on and leaf-off scenarios, as well as OAT sensitivity analysis of soil roughness under different gravimetric water

Table 1. MIMICS parameters and its one-at-a-time (OAT) changes.

Parameter	Baseline	Sensitivity change	Source
Leaf distribution	Uniform	Spherical, Planophile	Akerblom et al. 2018 (Figure 3h)
Leaf thickness (cm)	0.1	0.05, 0.013	MIMICS default parameter, mean value between default and literature (Sancho-Knapik et al. 2021)
Branch PDF (leaf-on)[a] Branch PDF (leaf-off)[a]	Sycamore $[\sin(\theta +30°)^{20°}]$	Hawthorn $[\sin(\theta +18°)^{20°}]$, Normal	LiDAR data spring–summer. Sycamore (Figure 3b) and Hawthorn (Figure 3d)
Gravimetric Water content (m^3/m^3)	0.45 (Wet environment)	0.05 (Very Dry), 0.25 (Dry), 0.65 (Very Wet)	Field data (Cooper et al. 2021; Stanley et al. 2023). Applying a linear change in gravimetric water content of leaf, trunk and soil.
Air and Soil Temperature (°C)	10	1, 20	
Soil roughness	1.0	0.5, 0.0	NA

a) Changes in 1st and 2nd order branch, 3rd to 6th assumed normal distribution.

content conditions. Linear changes in leaf, trunk and soil water content were based on previous research outcomes (Betsch et al. 2011; Köcher et al. 2009; Zhou et al. 2021). A one-way Analysis of Variance (ANOVA) was conducted to determine if differences in the total backscatter signal were significant ($\alpha = 0.05$) due to the changes in the first five aforementioned input parameters, for simulations at 4 GHz, 6 GHz and 8 GHz in both VV and VH polarization and between 20° and 45° (in 5° increments).

A two-way ANOVA was also performed to compare water content conditions (leaf, trunk and soil) against soil roughness. This statistical test assesses the effect of each variable (water content against soil roughness) and considers if there is any interaction between variables. For simulations with significant differences, the total backscatter was compared with the backscatter of each simulated scatter component (Figure 1) to determine the component with the greatest influence.

The baseline simulation comprises a Sycamore tree, the dominant species in the area, assuming a uniform leaf distribution and 1st and 2nd order branches exhibiting a PDF as detailed in Figure 3b. In terms of higher-order branches (i.e. 3rd–6th), a normal distribution was assumed. This was due to their tendency to distribute radially to their lower branch axis with narrower opening angles (Millet, Bouchard, and Édelin 1999) and their permanence in the tree depends on their efficiency in the photosynthesis process (Coder 2018). Ground data was parameterised based on multi-year observations (Section 2.1.2), with the mean soil and air temperature being set to 10°C and gravimetric water content in the environment (leaf, trunk and soil) to 0.45 m^3/m^3. Soil roughness was assumed to be slightly smooth (i.e. Root Mean Square [RMS] being equal to 1.0 cm). The baseline modelling results can be found in Appendix B for each scattering component, with Appendix C containing the baseline parameters obtained by TLS and Appendix D the LiDAR 3D model.

2.2.2. Seasonal and spatial resolution analysis

For this section, simulations for each tree in the 1-ha region for leaf-on and leaf-off periods were run. However, due to the large number of Sycamore trees present within the region, and due to computational limitations, only 50% of the Sycamore trees were used in the aggregation. The 50% were selected at random, to remove the potential for selection biases. Each simulation took place at the C-band range (4 GHz, 6 GHz and 8 GHz) for both VV and VH polarizations and between 20° and 45° in 5° increments.

For the temporal analysis, a one-way ANOVA was performed for each polarization (VV and VH) to determine if total backscatter differences were significant ($\alpha = 0.05$) between seasons across all the trees and incidence angles. A species comparison via a one-way ANOVA was conducted to assess if changes in mean total backscatter between the species were statistically significant. Additionally, in leaf-on and leaf-off scenarios, the one-way ANOVA test was performed to see if differences in simulated backscatter were significant as a result of changing incidence angle.

For the spatial resolution comparisons, the 1-ha region was spatially aggregated to simulate the spatial resolution of Sentinel-1 (approximately 20 m × 20 m). The spatial aggregation was completed by averaging the simulations for each tree within each individual pixel. The spatially averaged simulations were also compared to observations of Sentinel-1, taken on 25/12/15 and 01/01/16 (representing leaf-off conditions) and 05/07/15 and 10/07/15 (representing leaf-on conditions). To compare the simulations to the Sentinel-1 observations, the simulations took place at incidence angles close to the Sentinel-1 incidence angles observed over Wytham Woods (35° for simulated against 36° for observed and 45° for simulated against 43° for observed).

Sentinel-1 IW-GRDH (Interferometric Wide swath mode, Ground Range Detected) data was processed using ESA's Sentinel Application Platform (SNAP), to geolocate and calibrate the backscatter signal. The processing workflow is similar to that of Filipponi (2019), Maslanka et al. (2022), which includes applying an orbital correction, removing the thermal and boundary noise artefacts, applying radiometric calibrations, and applying a 'Refined-Lee' speckle filter, before applying terrain correction, using the Shuttle Radar Topography Mission (SRTM) 1 arc-second dataset. The resulting calibrated backscatter data was then reprojected to a 20 m by 20 m grid resolution, to match that of the MIMICS simulations, before being subset over the Wytham Woods region of interest. Only polarization modes VV and VH were used for comparison with the MIMICS model.

2.2.3. AGB estimation and relationship with backscatter

Allometric equations reported in the literature (Table 2) were used to calculate AGB using the data for each tree inside the 1-ha subset of Wytham Woods as reported by Terryn et al. (2020), except for Sycamore. To provide a consecutive set of tree heights for the Sycamore species, the selection of representative trees was obtained from a histogram of heights in 1-m step, resulting in a representation of 50%.

Simulated backscatter for VV and VH polarizations was compared to the calculated AGB (M_0, M_1, M_2 and M_3), and a regression model relating simulated C-band backscatter against each model was calculated. Although all the allometric models in Table 2 were developed for AGB estimation, they have been reported as unsuitable for Wytham Woods (Kim et al. 2022). Hence, co-polarized and cross-polarized backscatter was compared to AGB calculated using tree volume data (Terryn et al. 2020) and tree density (Kim et al. 2022).

Additionally, MIMICS input parameters (e.g. tree height and 1st order branch density) were compared with simulated backscatter to determine a possible relationship. Finally, field measurements, taken from the TLS data, such as DBH, tree height, tree volume, stem length, stem distance and crown height were compared with each other to provide relationships between variables.

Table 2. Allometric models to obtain the aboveground biomass.

Specie (Scientific Name)	Bunce (1968)[a]	Kim et al. (2022)[b]
Ash (Fraxinus excelsior)	$M_0 = e^{(-5.234459+2.480921*\ln(G))}$	$M_2 = e^{(0.84+1.9*\ln(D)+0.58*\ln(H))}$ $M_1 = e^{(2.98+2.30*\ln(D))}$
Hawthorn (Crataegus monogyna)		$M_3 = e^{(-1.76+1.34*\ln(D)+0.67*\ln(H)+0.48*\ln(CA))}$
Hazel (Corylus avellana)	$M_0 = e^{(-5.223864+2.425436*\ln(G))}$	
Oak (Quercus robur)	$M_0 = e^{(-5.501575+2.531795*\ln(G))}$	
Maple (Acer campestre)	$M_0 = e^{(-5.570499+2.529411*\ln(G))}$	
Unknown		
Sycamore (Acer pseudoplatanus)		$M_1 = e^{(3.15+2.42*\ln(D))}$
		$M_2 = e^{(0.78+2.05*\ln(D)+0.64*\ln(H))}$
		$M_3 = e^{(-1.34+1.52*\ln(D)+0.74*\ln(H)+0.36*\ln(CA))}$
Specie (Scientific Name)	Bunce (1968)[a]	Kim et al. (2022)[b]
Ash (Fraxinus excelsior)	$M_0 = e^{(-5.234459+2.480921*\ln(G))}$	$M_1 = e^{(2.98+2.30*\ln(D))}$
Hawthorn (Crataegus monogyna)		$M_2 = e^{(0.84+1.9*\ln(D)+0.58*\ln(H))}$
Hazel (Corylus avellana)	$M_0 = e^{(-5.223864+2.425436*\ln(G))}$	$M_3 = e^{(-1.76+1.34*\ln(D)+0.67*\ln(H)+0.48*\ln(CA))}$
Oak (Quercus robur)	$M_0 = e^{(-5.501575+2.531795*\ln(G))}$	
Maple (Acer campestre)	$M_0 = e^{(-5.570499+2.529411*\ln(G))}$	
Unknown		
Sycamore (Acer pseudoplatanus)		$M_1 = e^{(3.15+2.42*\ln(D))}$
		$M_2 = e^{(0.78+2.05*\ln(D)+0.64*\ln(H))}$
		$M_3 = e^{(-1.34+1.52*\ln(D)+0.74*\ln(H)+0.36*\ln(CA))}$

a) Combined locations. G = tree girth (m), derived from diameter at breast height.
b) Volume (m3) was converted to mass (kg) using density reported in supplementary table S2 in Kim et al. (2022). D= diameter at breast height (m), H = tree height (m) and CA = crown area (m^2).

3. Results

3.1. Sensitivity analysis

Table 3 shows the results of the one-way and two-way OAT ANOVA sensitivity tests as detailed in Section 2.2.1 and Table 1. Results are based on the 4 GHz simulations since the other two frequencies (6 GHz and 8 GHz) presented similar values (see Appendix B). The ANOVA analysis was performed to statistically evaluate differences in total backscatter means (from 20° to 45° in 5° increments) between baseline and simulated scenarios for co-polarized and cross-polarized modes. For the one-way OAT ANOVA, it was found that variations in total backscatter resulting from changes in soil roughness, air and soil temperature as well as 1st and 2nd order branch distributions in the leaf-on scenario were not

Table 3. *p*-values of the one-way and two-way ANOVA analyses for MIMICS model sensitivity to simulated backscatter at 4 GHz frequency of each polarization mode.

| Parameter	One-way ANOVA	
	VV	VH
Leaf distribution	p < 0.001*	p < 0.001*
Leaf thickness (cm)	p < 0.001*	p < 0.001*
Branch Distribution (leaf-on)	p > 0.050	p > 0.050
Branch Distribution (leaf-off)	p < 0.010*	p > 0.050
Temperature (°C)	p > 0.050	p > 0.050
Soil roughness (cm)[a]	p > 0.050	p > 0.050
Water content (m^3/m^3)	p < 0.001*	p < 0.001*
Two-way ANOVA		
Soil roughness (cm)	p > 0.050	p > 0.050
Water content (m^3/m^3)	p < 0.001*	p < 0.001*
Soil roughness and water content	p > 0.050	p > 0.050

a) Simulation with leaf, trunk and soil gravimetric water content of 0.45 m^3/m^3.
*Significant differences.

significant, in either the VV or VH simulations. However, for variations in the leaf orientation distribution and leaf thickness, in addition to the gravimetric water content in the leaf and trunk material, the OAT ANOVA suggests that differences in total backscatter were significant, in both the VV and VH polarizations. It was also found that the 1st and 2nd order branch distributions within the crown for the leaf-off scenario were significantly different for simulations in VV, but not in VH. For the two-way OAT ANOVA, it should be noted that whilst the gravimetric water content (leaf, trunk, and soil) does produce significant differences in total backscatter, the interactions between gravimetric water content and surface roughness do not produce significant differences in total backscatter.

As the direct crown backscatter was by far the most dominant component (Appendix E), the results from the OAT sensitivity analysis will show the backscatter variations of this component, and only for the variables found to have a significant backscatter difference, as observed in the ANOVA study (Table 3). Additionally, the simulations were similar for all frequencies simulated (4 GHz, 6 GHz, and 8 GHz, Appendix B), and thus subsequently only results from the 4 GHz simulations are shown.

Figure 4 shows the OAT simulations for the uniform leaf orientation distributions (the baseline simulation) against planophile and spherical orientations. It can be seen that, for the simulated direct crown backscatter in VV polarization, the planophile leaf distribution results in a greater change in backscatter with respect to incidence angle (-5.37 dB at 20°, -10.41 dB at 45°, and mean backscatter of -7.92 dB) compared to that of the uniform baseline simulation (-6.98 dB at 20°, -10.23 dB at 45°, and mean backscatter of -8.68 dB) and spherical leaf orientation (-8.95 dB at 20°, -9.92 dB at 45°, and mean backscatter of -9.33 dB), whereas the opposite is true for the cross-polarized (VH) simulations (planophile: -24.27 dB at 20°, -24.23 dB at 45°, and mean backscatter of -24.19 dB; uniform: -23.48 dB at 20°, -24.01 dB at 45°, and mean backscatter of -23.65 dB, spherical: -22.90 dB at 20°, -23.86 dB at 45°, and mean backscatter of -23.27 dB). Additionally, for both VV and VH simulations, the backscatter return for the simulations converges as the incidence angle increases from 20° to 45°.
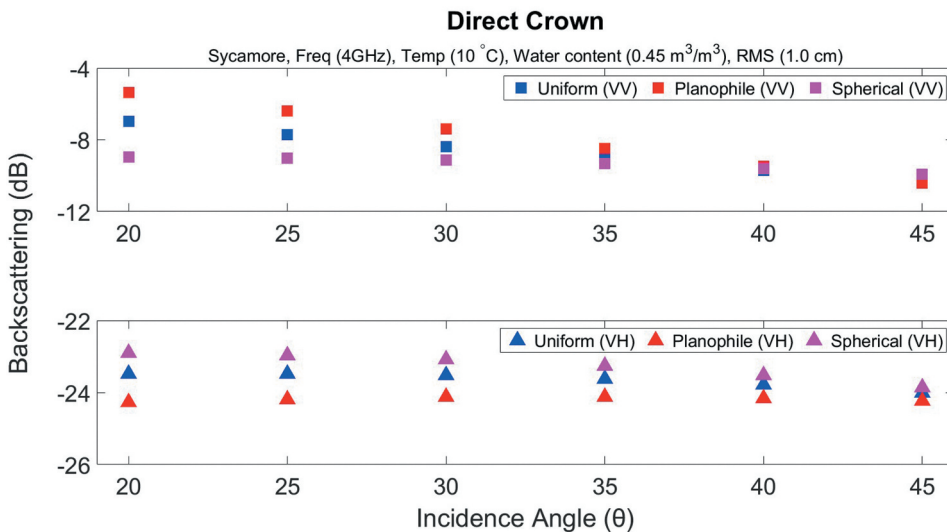
Figure 4. Direct from crown backscatter signal against antenna incidence angle for uniform (blue), planophile (red) and spherical leaves distribution (magenta) of co-polarised mode (VV, square) and cross-polarised mode (VH, triangle).
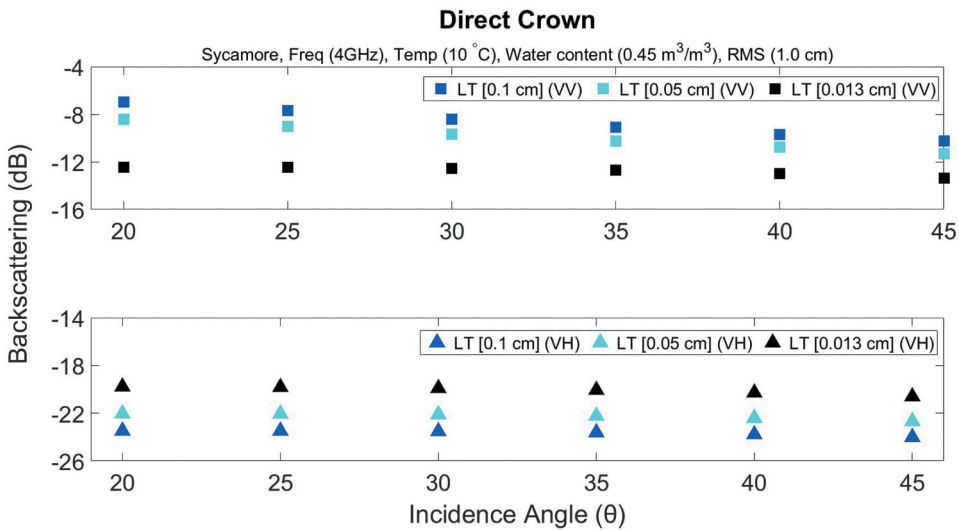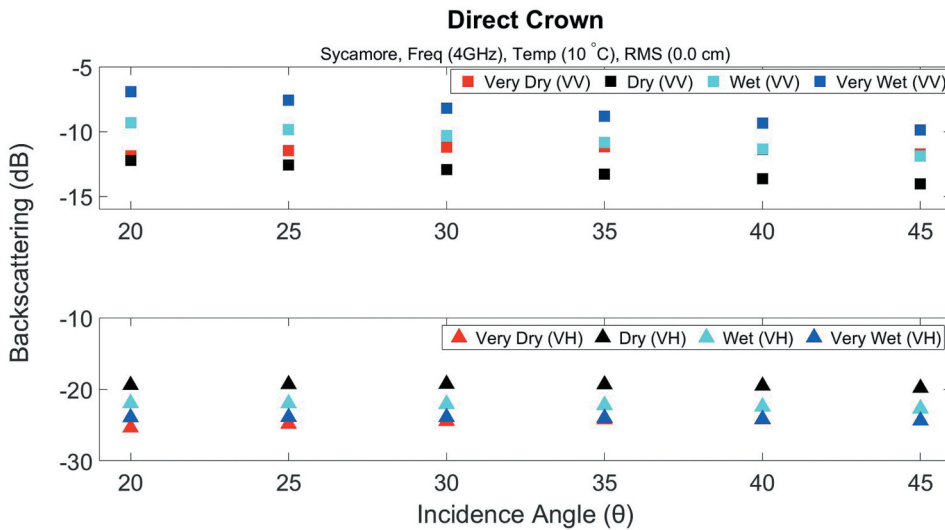
Figure 5. Direct from crown backscatter signal against antenna incidence angle for leaf thickness of 0.1 cm (blue), 0.05 cm (cyan) and 0.013 cm (black) of co-polarised mode (VV, square) and cross-polarised mode (VH, triangle).

Figure 5 shows the OAT simulations for the leaf thickness sensitivity tests. It was shown that, across all incidence angles, decreasing the leaf thickness decreases the backscatter of the direct crown VV simulations (e.g. −6.98 dB, −8.40 dB and −12.44 dB for leaf thicknesses of 0.1 cm, 0.05 cm and 0.013 cm, respectively, at 20°) but increases the backscatter for the direct crown VH simulations (−23.48 dB, −22.04 dB and −19.78 dB for leaf thicknesses of 0.1 cm, 0.05 cm and 0.013 cm, respectively, at 20°).

Figure 6 shows the OAT simulations for the gravimetric water content (leaf, trunk, and soil) sensitivity tests. Whilst for the co-polarization simulations there is a proportional reduction in backscatter with the decrement of gravimetric water content, the very dry scenario does not follow such a pattern. For example, backscatter in the very dry scenario exhibits higher values than those in the dry scenario. For the cross-polarized mode, backscatter increases proportionally with gravimetric water content except in the very dry scenario in which values are close to the very wet scenario.

3.2. Seasonal analysis

One-way ANOVA tests (Table 4) show that there was a significant difference in seasonality (spring–summer represented by leaf-on, autumn–winter represented by leaf-off respectively) in total backscatter (VV and VH) across all trees and incidence angles (Figure 7a). Regarding the effects of incidence angle on the simulated backscatter, for both seasons, Table 4 shows that backscatter differences between species in VV polarized at incidence angles less than and equal to 30°, in addition to 35° for the leaf-off simulations, were statistically significant. Contrarily, for VH-polarized simulations, differences in backscatter were not statistically significant for all incidence angles across both seasons, except for the leaf-off simulations at 45°.

Figure 6. Direct from crown backscatter signal against antenna incidence angle for very dry (red), dry (black), wet (cyan) and very wet (blue) scenarios of co-polarised mode (VV = square) and cross-polarised mode (VH = triangle). Scenarios are related to water content (m^3/m^3) of 0.05 for very dry, 0.25 for dry, 0.45 for wet (baseline) and 0.65 for very wet.

Table 4. p-values of ANOVA analysis for MIMICS seasonal analysis of the simulated backscatter 4 GHz frequency of each polarization mode.

One way ANOVA				
	VV		VH	
	$p < 0.001$*		$p < 0.001$*	
Season	Leaf-on (Spring–Summer)		Leaf-off (Autumn–Winter)	
	VV	VH	VV	VH
20°	$p < 0.050$*	$p > 0.050$	$p < 0.001$*	$p > 0.050$
25°	$p < 0.050$*	$p > 0.050$	$p < 0.001$*	$p > 0.050$
30°	$p < 0.050$*	$p > 0.050$	$p < 0.001$*	$p > 0.050$
35°	$p > 0.050$	$p > 0.050$	$p < 0.050$*	$p > 0.050$
40°	$p > 0.050$	$p > 0.050$	$p > 0.050$	$p > 0.050$
45°	$p > 0.050$	$p > 0.050$	$p > 0.050$	$p < 0.050$*

*Significant differences.

In all species, the simulated VV backscatter for leaf-on scenarios was larger than those for the leaf-off (Figure 7b). In contrast, in VH mode for leaf-on scenarios across all tree species, the simulated backscatter was smaller than in leaf-off scenarios (Figure 7c).

3.3. Spatial analysis

Figures 8 and 9 show the comparison of the spatial simulations for leaf-on and leaf-off scenarios with observations of summer and winter backscatter observations from Sentinel-1, respectively. For both seasons, observations were taken from two relative orbits (030 and 132) to get a range of incidence angles across Wytham Woods. A poor agreement was found
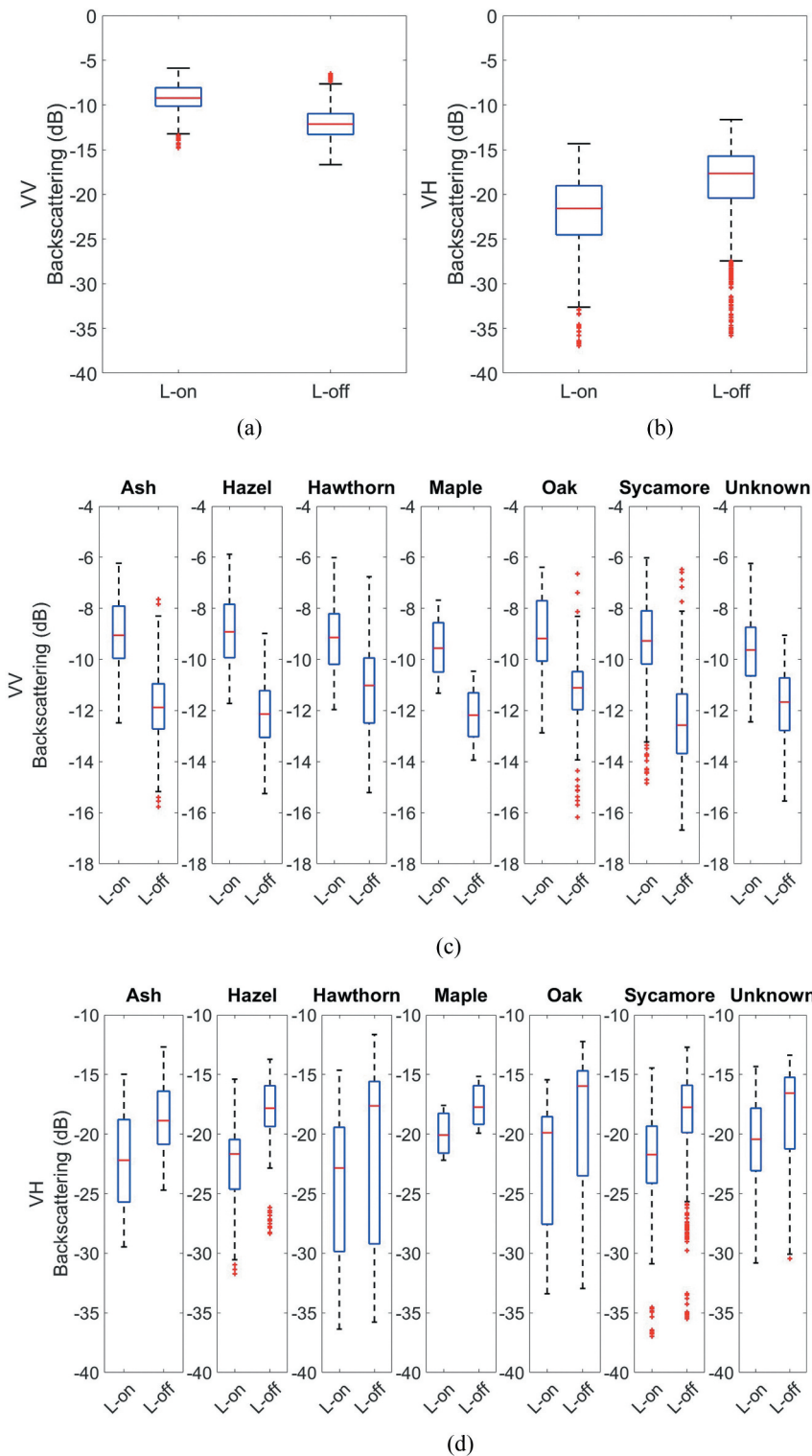
Figure 7. a) Backscatter box plot of all simulated trees at the 1-ha in spring-summer (leaf-on = L-on) and autumn-winter (leaf-off = L-off) periods, a) co-polarised mode (VV) and b) cross-polarised mode (VH). Backscatter box plot between species and seasonality c) co-polarised mode (VV) and d) cross-polarised mode (VH) backscatter box plot between species and seasonality. The red lines in the box plot represent the mean backscatter values, and whiskers the interquartile ranges.
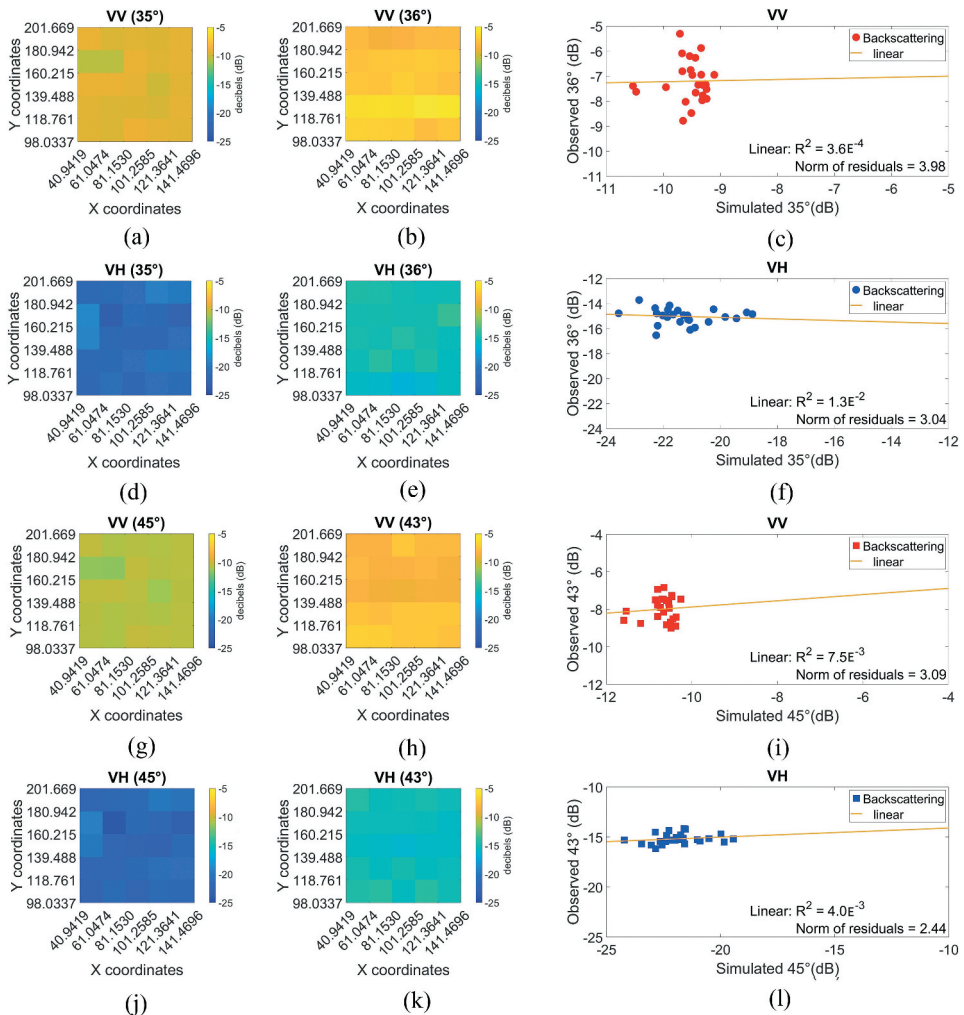
Figure 8. Backscatter simulations via MIMICS (a, d, g, j) and Sentinel-1 observations (b, e, h, k) for the 1-ha area in the leaf-on (spring-summer) scenario for both VV and VH polarisations. Sentinel-1 observations took place on 10/07/2015 (b, e) and 05/07/2015 (h, k). Scatter plot of simulated against observed data (c, f, i, l).

between simulated and observed backscatter under the 20 m × 20 m grid approach. The mean simulated backscatter across the 1-ha region underestimates the backscatter return when compared to the observations, regardless of polarization, seasonality, or incidence angle (Table 5). Higher differences were observed in the leaf-off (autumn–winter) than in leaf-on (spring–summer) scenarios.

3.4. Comparison of AGB against Backscatter

A strong relationship between TLS variables was observed (Figure 10), this is a good indicator of the role of structural tree elements (i.e. DBH and tree height) in tree volume, which is related to AGB.
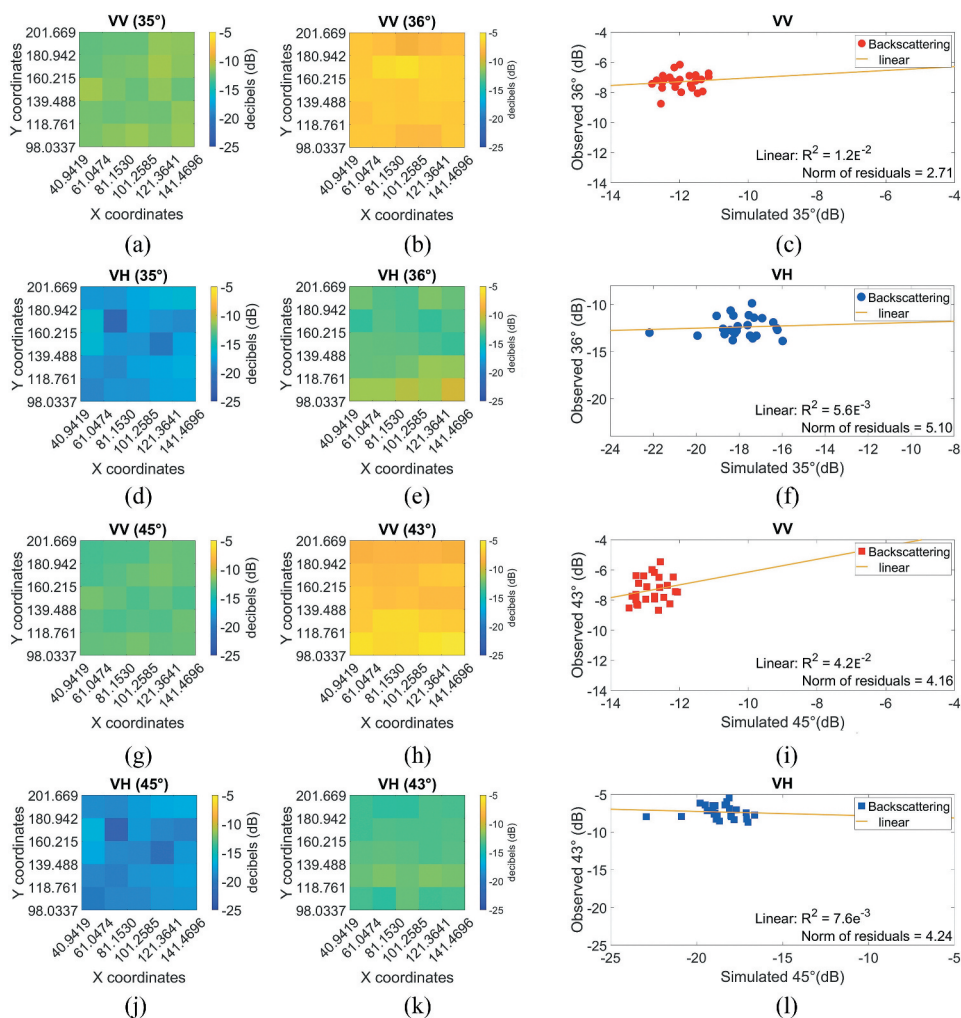
Figure 9. Backscatter simulations via MIMICS (a, d, g, j) and Sentinel-1 observations (b, e, h, k) for the 1-ha area in the leaf-off (autumn-winter) scenario for both VV and VH polarisations. Sentinel-1 observations took place on 01/01/2016 (b, e) and 25/12/15 (h, k). Scatter plot of simulated against observed data (c, f, i, l).

Table 5. Mean backscatter values for the MIMICS simulations and sentinel-1 observations, for both leaf-on and leaf-off scenarios, representing spring–summer and autumn–winter simulations, respectively, across the 1-ha region. Data have been aggregated from Appendix F.

Backscatter (dB)	Angle	Spring–Summer		Autumn–Winter	
		VV	VH	VV	VH
Simulated	35	−9.53	−21.28	−11.97	−17.94
Observed	36	−7.21	−15.03	−7.29	−12.40
Difference		−2.33	−6.25	−4.68	−5.54
Simulated	45	−10.68	−21.85	−12.80	−18.63
Observed	43	−7.99	−15.18	−7.33	−13.11
Difference		−2.69	−6.67	−5.47	−5.53
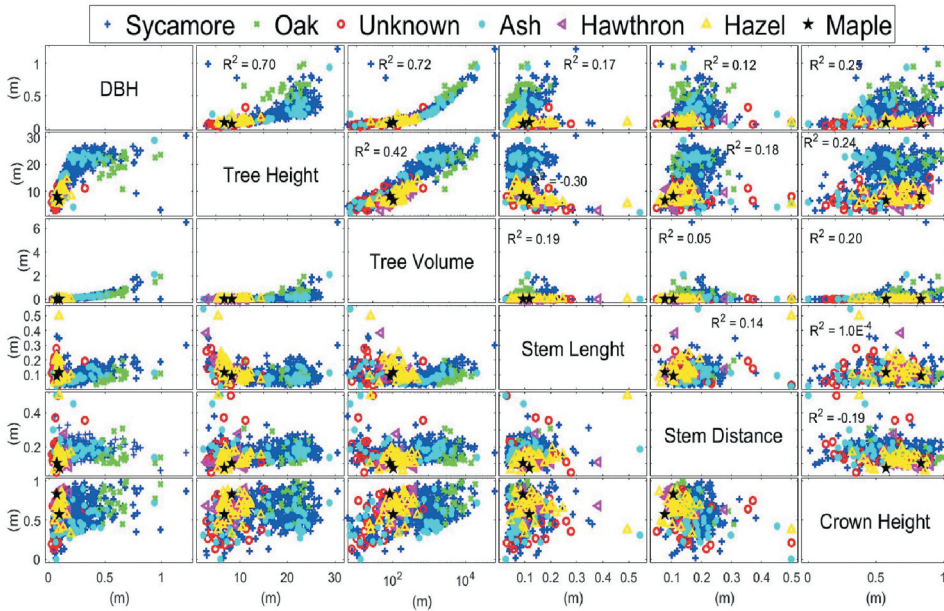
Figure 10. Parameters obtained in the latest field study at Wytham Woods, and their corresponding correlation coefficient to measure linear correlation between pairs.

AGB was calculated using all the allometric models in Table 2, using tree girth (derived from DBH), diameter at breast height (DBH), Tree Height (H) and Crown Area (CA) as recorded by the TLS, and was compared to leaf-on and leaf-off backscatter simulations of all the trees scanned within the 1-ha subregion. Simulations were performed in both VV- and VH-polarization, between 20° and 45°, in 5° increments. Table 6 shows the R^2 values between simulated backscatter and AGB at different incidence angles. Regardless of polarization or incidence angle, there was no correlation between simulated backscatter and any of the allometric equations and AGB-TLS (AGB calculated using tree volume derived from TLS), with all R^2 values being less than 0.5. Nonetheless, AGB-TLS presented slightly better agreement than allometric models. Figure 11 shows AGB-TLS against backscatter simulations taking place at 35° corresponding to one of the incidence angles experienced by Sentinel-1 over the 1-ha region of Wytham Woods.

The R^2 values were also calculated between simulated backscatter and crown thickness, trunk length, leaf density (leaf-on simulations) and 1st-order branch density (leaf-off simulations). Regardless of polarization or incidence angle, there was no correlation between simulated backscatter, and any of the tested variables, with all R^2 values being less than 0.5 (Appendix G). However, it should be noted that there was slightly better agreement between leaf density and backscatter in leaf-on simulations as well as between branch density and backscatter in leaf-off simulations, compared with AGB and simulated backscatter. This is to be expected as the direct crown contribution to the total backscatter was found to be dominant at C-band frequencies (e.g. 4 GHz, see Appendix E).

Table 6. Coefficient of determination (R2) of each allometric model against simulated backscatter at different incidence angles for the two polarization modes and both seasonal scenarios.

Angle($\theta°$)	R^2 (Leaf-on simulations)									
	M_0		M_1		M_2		M_3		AGB-TLS[a]	
	VV	VH	VV	VH	VV	VH	VV	VH	VV	VH
20	1.1E-04	4.0E-03	2.6E-05	4.4E-03	4.8E-05	6.6E-04	5.2E-05	2.7E-03	2.9E-03	4.7E-02
25	1.3E-03	4.8E-03	9.4E-04	5.3E-03	8.8E-04	1.2E-03	1.9E-04	3.8E-03	2.7E-03	4.1E-02
30	3.9E-03	5.5E-03	3.3E-03	6.1E-03	3.2E-03	2.0E-03	1.5E-03	5.1E-03	3.6E-03	3.4E-02
35	7.5E-03	6.1E-03	6.8E-03	6.7E-03	7.1E-03	2.8E-03	5.5E-03	6.7E-03	3.1E-03	3.0E-02
40	9.3E-03	6.5E-03	8.7E-03	7.2E-03	9.4E-03	3.5E-03	8.0E-03	8.2E-03	3.9E-03	2.7E-02
45	8.6E-03	6.8E-03	8.1E-03	7.5E-03	9.4E-03	4.1E-03	7.9E-03	9.5E-03	5.7E-03	2.5E-02
Angle($\theta°$)	R^2 (Leaf-off simulations)									
	M_0		M_1		M_2		M_3		AGB-TLS	
	VV	VH	VV	VH	VV	VH	VV	VH	VV	VH
20	6.0E-03	1.7E-03	5.3E-03	1.8E-03	8.3E-04	3.7E-04	2.6E-03	2.1E-03	9.7E-02	1.7E-02
25	9.2E-03	2.2E-03	8.6E-03	2.3E-03	3.6E-05	8.3E-04	4.1E-04	3.1E-03	5.9E-02	1.4E-02
30	1.2E-02	2.8E-03	1.1E-02	2.9E-03	1.3E-03	1.5E-03	1.2E-04	4.3E-03	3.1E-02	1.0E-02
35	1.4E-02	3.2E-03	1.4E-02	3.4E-03	4.1E-03	2.1E-03	2.8E-03	5.8E-03	2.6E-02	8.4E-03
40	1.5E-02	3.5E-03	1.5E-02	3.7E-03	6.0E-03	2.7E-03	5.3E-03	7.2E-03	1.8E-02	7.2E-03
45	1.4E-02	3.7E-03	1.4E-02	3.9E-03	6.9E-03	3.2E-03	6.4E-03	8.3E-03	1.1E-02	6.1E-03

a) AGB (t m^{-2}) calculated using tree volume data (Terryn et al. 2020) and tree density (Kim et al. 2022).
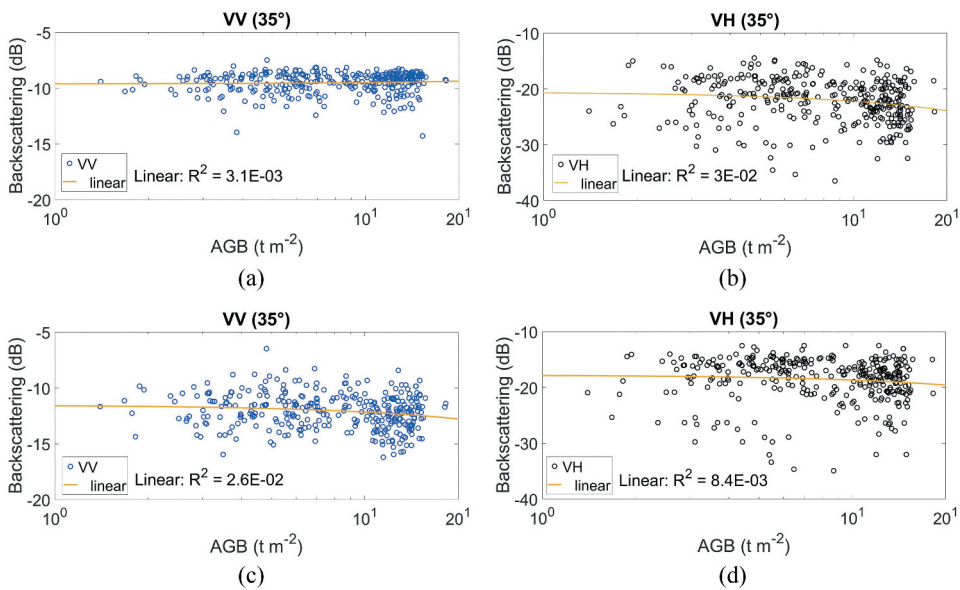
Figure 11. Comparison of calculated AGB-TLS against simulated backscatter at incidence angles of 35°. Spring-summer season (leaf-on simulations) a) co-polarised (VV) and b) cross-polarised (VH). Autumn-winter season (leaf-off simulations) c) co-polarised (VV) and d) cross-polarised (VH).

4. Discussion

The sensitivity analysis described in Section 2.2 allows to understand the variability of the simulated backscatter (VV and VH) in relation to changes in the value of the input

parameters. The OAT test showed that there were significant differences in the direct-crown backscatter contribution (the dominant contribution to total backscatter) when altering the leaf orientation, leaf thickness, and gravimetric water content (leaf, trunk, and soil). This is to be expected for the leaf variable changes (orientation and thickness), given that at the C-band, the radar backscatter is highly influenced by the crown components. Model sensitivity to leaf distribution suggests that assumptions related to leaf orientation will lead to statistically significant differences in backscatter return, especially at incidence angles of <30°. At incidence angles of ≥30°, the differences are not as significant, suggesting that the orientation of the leaf is not as important for most of the Sentinel-1 IW swath (Sentinel-1 swath incidence angle ranges from 29.1° to 46.0°). Nonetheless, leaf orientation distribution for each tree can be related to many factors. For example, leaves can be oriented to increase light exposure, which is crucial for photosynthesis (Posada et al. 2012). Additionally, these angles can change during the day (Nilsen and Forseth 2018). Furthermore, in dense forests such as Wytham Woods, the angles of the leaves might vary allowing them to avoid being covered by other leaves, assuring them to receive sufficient light (Miyata and Kohyama 2016). All of these highlight the diversity in leaf orientation that can occur in individual trees regardless of the species and in turn the effect on the scattering mechanism impacting biomass predictions due to the assumption of a linear backscatter–biomass relationship. The outcomes obtained in our research by modelling backscatter under changes in leaf orientation encourage a better *in-situ* characterization of this leaf parameter in forests, and several attempts have been made under the development of optical instruments (Lolli et al. 2014) and TLS software (Stovall et al. 2021); however, these approaches are limited to small areas, so further research covering larger areas is recommended to increase leave orientation samples and thus better characterize their variability in trees. Furthermore, since direct knowledge of leaf orientation, is not possible under current satellite technology, RT models can also be applied for the development of new satellite instruments with more sensitivity to canopy scattering mechanisms (Pan, Pierce, and Moghaddam 2005).

Leaf thickness sensitivity analysis showed a relationship between leaf thickness and backscatter (increasing/decreasing backscatter for increasing/decreasing leaf thickness at VV/VH polarizations). MIMICS calculates leaf scattering assuming an electric current sheet of complex resistivity, which depends on leaf thickness and dielectric material, with the latter depending on water content (Ulaby et al. 1990b). Simulations were done by varying the leaf thickness and assuming the same dielectric material; therefore, the interaction between these two variables was not considered. However, it should be noted that in nature, variation of the leaf thickness may have a direct effect on the water content and indirectly on the dielectric change (Ulaby and Jedlicka 1984). Hence, care must then be taken when entering values of leaf thickness and its corresponding dielectric material values for accurate backscatter simulation. Also, depending on the elevation of leaves in the canopy, their thickness can vary significantly, with thicker leaves higher in the canopy exposing them more to light (Koike et al. 2001). Furthermore, variability in leaf thickness from the same species in deciduous forests has been reported (da Silva, Helena Porfírio, and Rodrigo Rossatto 2024), and additionally, leaf morphology can be related to environmental stress adaptation such as water scarcity or high temperature (Cao et al. 2024). Our findings show that changes in leaf thickness have important differences in the simulated

backscatter, suggesting that biomass estimation from satellite data and under the assumption of AGB-backscatter linearity can lead to errors in the predictions of forest biomass especially in those subject to environmental stresses due to climate change. Hence, it is important to understand the effect of this parameter in the backscatter responses under modelling approaches.

Mathematical models are a simplification of reality; the results from MIMICS sensitivity analysis assessed parameters and changes where a statistically significant effect was observed on simulated backscatter. We found that this information is limited in the literature from the available RT models, including MIMICS. Hence, the backscatter effects between these models could vary depending on the parameters or their change in value (Bosisio and Dechambre 2010) or between modelling approaches (i.e. radiative transfer theory or distorted Bron approximation, Saatchi and McDonald 1997). Nonetheless, our findings promote two possible applications. a) sensitivity analysis comparison between RT models and modelling approaches and b) experimental settings in both the laboratory (Morrison et al. 2001) or *in-situ* (Morrison, Bennett, and Solberg 2013) with the addition of parameter measurements (i.e. leaf orientation; leaf thickness; and gravimetric water content in leaf, trunk, and soil) for a quantitative comparison with backscatter changes.

The seasonal analysis showed that there was a significant difference when comparing the leaf-on and leaf-off (i.e. spring–summer and autumn–winter) backscatter simulations at both polarizations. This is to be expected, given that the direct crown is the most dominant contributor in the total backscatter at C-band frequencies. Previous studies at L-band frequencies (Pan, Pierce, and Moghaddam 2005) have shown that MIMICS simulations were dominated by ground–trunk contributions (contributor 6 in Figure 1) for leaf-off simulations of backscatter. This was not found to be the case for the leaf-on C-band simulations in this study, primarily due to the C-band's inability to penetrate through the canopy as deeply as L-band frequencies (de Jesus, Batista, and Mora Kuplich 2020; Omar, Misman, and Kassim 2017). When the leaves were removed (i.e. going from leaf-on to leaf-off), the backscatter signal changed significantly, as the main source of the backscatter signal (leaves) was removed, and the other elements (branches) became more dominant within the total backscatter signal. Seasonality was previously found to be an important factor when classifying tree species with space-based SAR observations (Borlaf-Mena et al. 2023). Our seasonal results highlighted that differences are only important in co-polarized (VV) mode at incidence angles less than and equal to 30° (Table 4). Furthermore, the findings support the use of the C-band radar from satellite data to track seasonal changes in forests, which at the same time has potential implications for understanding forest dynamics (Soudani et al. 2021) and ecological processes (Wismann, Boehnke, and Schmullius 1995).

The spatial analysis shows that the simulated backscatter for both leaf-on and leaf-off scenarios (for both VV- and VH-polarizations) underestimated the backscatter of the 1-ha region when compared to the observations from Sentinel-1. The difference between the mean simulated and mean observed backscatter increased with increasing incidence angle, for both the leaf-on and leaf-off scenarios, with the VH-polarization differences being greater than those for VV-polarization. This general underestimation can be related to MIMICS's use of a uniform-forest layer which does not consider multiple scattering from different layers of the crowns – a crown–crown contribution (Pan et al. 2005). Moreover, RT

models based on the individual tree approach have shown better agreement with satellite data (Guoqing and Jon Ranson 1995). The underrepresentation of Sycamore trees (50%) within the spatially binned and averaged data may have artificially reduced the simulated backscatter when compared to the observations. However, a random sampling method was contemplated for Sycamore tree simulations as part of this study to reduce such errors. However, the findings could also be an indicator of the potential implication of the low spatial resolution from satellite data, restricting the understanding of the role that individual trees play in the backscatter signal of the scanned area (e.g. 20 m × 20 m). Ground-based radar systems and corresponding process signals (e.g. upscaling) can be a potential approach to investigate satellite data uncertainty due to its coarse spatial resolution.

It was also shown that there was no correlation between AGB models and simulated backscatter for the leaf-on simulations (R^2 << 0.5, Table 6); an expected result due to the inability of the C-band to penetrate through the leafy canopy. A better agreement was expected by removing the leaves, which are one of the structural elements that prevents signal penetration. However, this leaf-off scenario also presented a lack of correlation between AGB and simulated backscatter. Similar non-correlation outcomes have been observed in other models (Ranson et al. 1997). Although this no-linearity can be attributed to low signal penetrability from the C-band (i.e. a signal mainly 'sees' tree crown), under lower frequencies (S-band), a low correlation when comparing AGB from airborne SAR observations against backscatter simulation has also been reported (Ningthoujam et al. 2016). Furthermore, similar results (AGB-backscatter nonlinearity) have been found using satellite data in combinations of low and high frequencies, such as L- and X-band (Englhart, Keuck, and Siegert 2011) and C- and X-band (Xiaodong et al. 2018). The above emphasizes the nondirect linearity between AGB and backscatter, which can be due to tree structural complexity, water content variability (leaf, trunk and soil) or a combination of them. Multi-frequency (Santi et al. 2017) and polarimetric approaches (Zeng et al. 2022) have been developed to address these challenges. However, the restricted satellite missions with these sensor capabilities limit the application areas, and the complex data processing restricts knowledge of AGB from backscatter signals. Nonetheless, modelling approaches can compensate for these issues.

It should be noted that the estimations of AGB come from commonly used allometric equations derived from TLS measurements; the measurements may contain random errors that introduce uncertainty into the estimations, hence affecting the relationship with the backscatter signal. Nonetheless, the allometric models applied in this study (i.e. M0 in Bunce (1968) and M1, M2 and M3 in Kim et al. (2022)), were shown to be unsuitable for this Wytham Woods 1-ha area, which has been previously addressed by Kim et al. (2022). Additionally, the AGB calculated by TLS tree volume did not produce a meaningful relationship with the simulated C-band backscatter. The previous emphasizes that backscatter intensity is not proportional to biomass (Woodhouse et al. 2012) and suggests that vegetation structures have a significant effect on the signal return. Moreover, no relationship was found between C-band backscatter and either of the vegetation structure parameters (Appendix G) and likewise at lower frequencies (S-band, Ningthoujam et al.

2016), suggesting a more complex role of this feature in the backscatter signal. These results strongly support the need for more accurate allometric models to better assess the relationship between AGB and C-band signal backscatter. Additionally, we suggest the use of new technology such as UAV radar systems in conjunction with TLS for a better understanding of the AGB–backscatter relationship.

5. Conclusion

Simulations of the total backscatter using MIMICS in the C-band frequency range showed, as expected, that scattering directly from tree crowns is the main contribution element to the backscatter signal in both polarization modes. Sensitivity analyses presented important differences in those parameters presented in the crown, such as leaf distribution, leaf thickness and water content (leaf, trunk and soil). In terms of seasonal simulations, spring–summer (leaf-on) and autumn–winter (leaf-off), results showed larger values of simulated co-polarized backscatter in leaf-on scenarios than in leaf-off scenarios; an opposite behaviour was observed in the simulated cross-polarized backscatter. Additionally, important backscatter differences were observed in the 1-ha area (20 m × 20 m grid resolution) between simulated data and satellite data, in which the satellite presented the highest values. Finally, the calculated AGB under different allometric models did not show a relationship with the backscatter signal, suggesting high variability between AGB and backscatter in the C-band as well as the development of better allometric models to obtain forest biomass.

Disclosure statement

No potential conflict of interest was reported by the author(s).

ORCID

Veronica Escobar-Ruiz ⓘD http://orcid.org/0000-0003-1336-0921
Keith Morrison ⓘD http://orcid.org/0000-0002-8075-0316

Data availability statement

The data that support the findings of this study are available from the corresponding author, Escobar-Ruiz V., upon reasonable request.

References

Akerblom, M., P. Raumonen, E. Casella, M. I. Disney, F. M. Danson, R. Gaulton, L. A. Schofield, and M. Kaasalainen. 2018. "Non-Intersecting Leaf Insertion Algorithm for Tree Structure Models." *Interface Focus* 8 (2). https://doi.org/10.1098/rsfs.2017.0045 .

Badreldin, N., and A. Sanchez-Azofeifa. 2015. "Estimating Forest Biomass Dynamics by Integrating Multi-Temporal Landsat Satellite Images with Ground and Airborne LiDAR Data in the Coal Valley Mine, Alberta, Canada." *Remote Sensing* 7 (3): 2832–2849. https://doi.org/10.3390/rs70302832.

Balzter, H., C. Rowland, and P. Saich. 2007. "Forest Canopy Height and Carbon Estimation at Monks Wood National Nature Reserve, UK, Using Dual-Wavelength SAR Interferometry." *Remote Sensing of Environment* 108 (3): 224–239. https://doi.org/10.1016/j.rse.2006.11.014.

Betsch, P., D. Bonal, N. Breda, P. Montpied, M. Peiffer, A. Tuzet, and A. Granier. 2011. "Drought Effects on Water Relations in Beech: The Contribution of Exchangeable Water Reservoirs." *Agricultural and Forest Meteorology* 151 (5): 531–543. https://doi.org/10.1016/j.agrformet.2010.12.008.

Borlaf-Mena, I., J. García-Duro, M. Santoro, L. Villard, O. Badea, and M. Andrei Tanase. 2023. "Seasonality and Directionality Effects on Radar Backscatter are Key to Identify Mountain Forest Types with Sentinel-1 Data." *Remote Sensing of Environment* 296. https://doi.org/10.1016/j.rse.2023.113728.

Bosisio, A. V., and M. Dechambre. 2010. "Predictions of Microwave Attenuation Through Vegetation: A Comparison with Measurements." *International Journal of Remote Sensing* 25 (19): 3973–3997. https://doi.org/10.1080/01431160310001657524.

Bourbigot, M., J. Harald, P. Riccardo, and G. Hajduch. 2016. Sentinel-1 Product Definition 2016. 15 Feb 2024 https://sentinels.copernicus.eu/documents/247904/1877131/Sentinel-1-Product-Definition.pdf/6049ee42-6dc7-4e76-9886-f7a72f5631f3?t=1461673251000 .

Bunce, R. G. H. 1968. "Biomass and Production of Trees in a Mixed Deciduous Woodland: I. Girth and Height as Parameters for the Estimation of Tree Dry Weight." *The Journal of Ecology* 56 (3): 3. https://doi.org/10.2307/2258105.

Butt, N., G. Campbell, Y. Malhi, M. Morecroft, K. Fenn, M. Thomas. 2009. *Initial results from establishment of a long-term broadleaf monitoring plot at Wytham Woods*. Oxford, UK: University Oxford.

Calders, K., G. Newnham, A. Burt, S. Murphy, P. Raumonen, M. Herold, D. Culvenor, et al. 2014. "Nondestructive Estimates of Above-Ground Biomass Using Terrestrial Laser Scanning." *Methods in Ecology and Evolution* 6 (2): 198–208. https://doi.org/10.1111/2041-210x.12301.

Calders, K., N. Origo, A. Burt, M. Disney, J. Nightingale, P. Raumonen, M. Åkerblom, Y. Malhi, and P. Lewis. 2018. "Realistic Forest Stand Reconstruction from Terrestrial LiDAR for Radiative Transfer Modelling." *Remote Sensing* 10 (6): 933. https://doi.org/10.3390/rs10060933.

Cao, C., S. Cui, X. Guan, Y. Chen, Y. Zhang, X. Lin, C. Wu, et al. 2024. "Plant Leaf Functional Adaptions Along Urban–Rural Gradients of Jinhua City." *Plants (Basel)* 13 (12): 1586. https://doi.org/10.3390/plants13121586.

Chuah, H. T., and H. S. Tan. 1992. "A Radar Backscatter Model for Forest Stands." *Waves in Random Media* 2 (1): 7–28. https://doi.org/10.1088/0959-7174/2/1/002.

Chung, W., P. Evangelista, N. Anderson, A. Vorster, H. Han, K. Poudel, and R. Sturtevant. 2017. "Estimating Aboveground Tree Biomass for Beetle-Killed Lodgepole Pine in the Rocky

Mountains of Northern Colorado." *Forest Science* 63 (4): 413–419. https://doi.org/10.5849/fs.2016-065.

Coder, K. D. 2018. "Tree Anatomy: Shoots and Growth Patterns." In *Warnell School of Forestry & Natural Resources*, edited by O. Publication, 18. Georgia, United States: University of Georgia.

Cooper, H. M., E. Bennett, J. Blake, E. Blyth, D. Boorman, E. Cooper, J. Evans, et al. 2021. "COSMOS-UK: National Soil Moisture and Hydrometeorology Data for Environmental Science Research." *Earth System Science Data* 13 (4): 1737–1757. https://doi.org/10.5194/essd-13-1737-2021.

Cranfield University. 2024. "The Soils Guide." Cranfield University. Accessed by February 23. www.landis.org.uk .

da Silva, B. Helena Porfírio, and D. Rodrigo Rossatto. 2024. "Leaf Tolerance to Heat is Independent of Leaf Phenology in Neotropical Savanna Trees." *Trees*. https://doi.org/10.1007/s00468-024-02547-0.

de Jesus, J. Batista, and T. Mora Kuplich. 2020. "Applications of Sar Data to Estimate Forest Biophysical Variables in Brazil." *Cerne* 26 (1): 88–97. https://doi.org/10.1590/01047760202026012656.

de Jesus, B. Janisson, M. K. Tatiana, Í. D. de C Barreto, F. L. Hillebrand, and N. C. da Rosa. 2023. "Estimation of Aboveground Biomass of Arboreal Species in the Semi-Arid Region of Brazil Using SAR (Synthetic Aperture Radar) Images." *Journal of Arid Land* 15 (6): 695–709. https://doi.org/10.1007/s40333-023-0017-4.

de Tanago, G., A. L. Jose, H. Bartholomeus, M. Herold, V. Avitabile, P. Raumonen, C. Martius, et al. 2017. "Estimation of Above-Ground Biomass of Large Tropical Trees with Terrestrial LiDAR." *Methods in Ecology and Evolution* 9 (2): 223–234. https://doi.org/10.1111/2041-210x.12904.

Englhart, S., V. Keuck, and F. Siegert. 2011. "Aboveground Biomass Retrieval in Tropical Forests — the Potential of Combined X- and L-Band SAR Data Use." *Remote Sensing of Environment* 115 (5): 1260–1271. https://doi.org/10.1016/j.rse.2011.01.008.

Filipponi, F. 2019. "Sentinel-1 GRD Preprocessing Workflow." *Proceedings* 18 (1): 11. https://doi.org/10.3390/ECRS-3-06201.

Grover, K., S. Quegan, and C. da Costa Freitas. 1999. "Quantitative Estimation of Tropical Forest Cover by SAR." *IEEE Transactions on Geoscience & Remote Sensing* 37 (1): 479–490. https://doi.org/10.1109/36.739096.

Guoqing, S., and K. Jon Ranson. 1995. "A Three-Dimensional Radar Backscatter Model of Forest Canopies." *IEEE Transactions on Geoscience & Remote Sensing* 33 (2): 372–382. https://doi.org/10.1109/36.377937.

Hethcoat, M. G., J. M. B. Carreiras, D. P. Edwards, R. G. Bryant, and S. Quegan. 2021. "Detecting Tropical Selective Logging with C-Band SAR Data May Require a Time Series Approach." *Remote Sensing of Environment* 259. https://doi.org/10.1016/j.rse.2021.112411.

Hubau, W., S. L. Lewis, O. L. Phillips, K. Affum-Baffoe, H. Beeckman, A. Cuni-Sanchez, A. K. Daniels, et al. 2020. "Asynchronous Carbon Sink Saturation in African and Amazonian Tropical Forests." *Nature* 579 (7797): 80–87. https://doi.org/10.1038/s41586-020-2035-0.

Imhoff, M. L. 1995. "Radar Backscatter and Biomass Saturation: Ramifications for Global Biomass Inventory." *IEEE Transactions on Geoscience & Remote Sensing* 33 (2): 511–518. https://doi.org/10.1109/tgrs.1995.8746034.

Karam, M. A., F. Amar, A. K. Fung, E. Mougin, A. Lopes, D. M. Le Vine, and A. Beaudoin. 1995. "A Microwave Polarimetric Scattering Model for Forest Canopies Based on Vector Radiative Transfer Theory." *Remote Sensing of Environment* 53 (1): 16–30. https://doi.org/10.1016/0034-4257(95)00048-6.

Karam, M. A., and A. K. Fung. 1988. "Electromagnetic Scattering from a Layer of Finite Length, Randomly Oriented, Dielectric, Circular Cylinders Over a Rough Interface with Application to Vegetation." *International Journal of Remote Sensing* 9 (6): 1109–1134. https://doi.org/10.1080/01431168808954918.

Kim, C., H. Verbeeck, A. Burt, N. Origo, J. Nightingale, Y. Malhi, P. Wilkes, P. Raumonen, R. G. H. Bunce, and M. Disney. 2022. "Laser Scanning Reveals Potential Underestimation of Biomass Carbon in Temperate Forest." *Ecological Solutions and Evidence* 3 (4). https://doi.org/10.1002/2688-8319.12197.

Köcher, P., T. Gebauer, V. Horna, and C. Leuschner. 2009. "Statut hydrique des feuilles et flux xylèmique dans le tronc en relation avec la sécheresse du sol pour cinq espèces d'arbres feuillus tempérés à stratégies de consommation d'eau différentes." *Annals of Forest Science* 66 (1): 101–101. https://doi.org/10.1051/forest/2008076.

Koike, T., M. Kitao, Y. Maruyama, S. Mori, and T. T. Lei. 2001. "Leaf Morphology and Photosynthetic Adjustments Among Deciduous Broad-Leaved Trees within the Vertical Canopy Profile." *Tree Physiology* 21 (12–13): 951–958. https://doi.org/10.1093/treephys/21.12-13.951.

Kumar, L., and O. Mutanga. 2017. "Remote Sensing of Above-Ground Biomass." *Remote Sensing* 9 (9). https://doi.org/10.3390/rs9090935.

Lang, R. H., and J. S. Sighu. 1983. "Electromagnetic Backscattering from a Layer of Vegetation: A Discrete Approach." *IEEE Transactions on Geoscience & Remote Sensing* GE-21 (1): 62–71. https://doi.org/10.1109/tgrs.1983.350531.

Le Toan, T., A. Beaudoin, J. Riom, and D. Guyon. 1992. "Relating Forest Biomass to SAR Data." *IEEE Transactions on Geoscience & Remote Sensing* 30 (2): 403–411. https://doi.org/10.1109/36.134089.

Liu, Y. Y., A. I. J. M. van Dijk, R. A. M. de Jeu, J. G. Canadell, M. F. McCabe, J. P. Evans, and G. Wang. 2015. "Recent Reversal in Loss of Global Terrestrial Biomass." *Nature Climate Change* 5 (5): 470–474. https://doi.org/10.1038/nclimate2581.

Lolli, L., M. Pisani, M. Rajteri, J.-L. Widlowski, A. Bialek, C. Greenwell, and N. Fox. 2014. "Phytos: A Portable Goniometer Forin Situspectro-Directional Measurements of Leaves." *Metrologia* 51 (6): SS309–SS313. https://doi.org/10.1088/0026-1394/51/6/s309.

Lu, D., Q. Chen, G. Wang, L. Liu, G. Li, and E. Moran. 2014. "A Survey of Remote Sensing-Based Aboveground Biomass Estimation Methods in Forest Ecosystems." *International Journal of Digital Earth* 9 (1): 63–105. https://doi.org/10.1080/17538947.2014.990526.

Lu, D., Q. Chen, G. Wang, E. Moran, M. Batistella, M. Zhang, G. Vaglio Laurin, and D. Saah. 2012. "Aboveground Forest Biomass Estimation with Landsat and LiDAR Data and Uncertainty Analysis of the Estimates." *International Journal of Forestry Research* 2012:1–16. https://doi.org/10.1155/2012/436537.

Malhi, Y., P. Meir, and S. Brown. 2002. "Forests, Carbon and Global Climate." *Philosophical Transactions Series A, Mathematical, Physical, and Engineering Sciences* 360 (1797): 1567–1591. https://doi.org/10.1098/rsta.2002.1020.

Maslanka, W., K. Morrison, K. White, A. Verhoef, and J. Clark. 2022. "Retrieval of Sub-Kilometric Relative Surface Soil Moisture with Sentinel-1 Utilizing Different Backscatter Normalization Factors." *IEEE Transactions on Geoscience & Remote Sensing* 60:1–13. https://doi.org/10.1109/tgrs.2022.3175256.

Millet, J., A. Bouchard, and C. Édelin. 1999. "Relationship Between Architecture and Successional Status of Trees in the Temperate Deciduous Forest." *Écoscience* 6 (2): 187–203. https://doi.org/10.1080/11956860.1999.11682520.

Mitchard, E. T. A., S. S. Saatchi, L. J. T. White, K. A. Abernethy, K. J. Jeffery, S. L. Lewis, M. Collins, et al. 2012. "Mapping Tropical Forest Biomass with Radar and Spaceborne LiDAR in Lopé National Park, Gabon: Overcoming Problems of High Biomass and Persistent Cloud." *Biogeosciences* 9 (1): 179–191. https://doi.org/10.5194/bg-9-179-2012.

Miyata, R., and T. S. Kohyama. 2016. "Light-Exposed Shoots of Seven Coexisting Deciduous Species Show Common Photosynthetic Responses to Tree Height." *Oecologia* 182 (2): 373–383. https://doi.org/10.1007/s00442-016-3664-8.

Morrison, K., J. C. Bennett, G. Cookmartin, A. J. McDonald, A. Race, and S. Quegan. 2001. "Three-Dimensional X-Band SAR Imaging of a Small Conifer Tree." *International Journal of Remote Sensing* 22 (4): 705–710. https://doi.org/10.1080/01431160010013487.

Morrison, K., J. Bennett, and S. Solberg. 2013. "Ground-Based C-Band Tomographic Profiling of a Conifer Forest Stand." *International Journal of Remote Sensing* 34 (21): 7838–7853. https://doi.org/10.1080/01431161.2013.826836.

Nilsen, E. T., and I. N. Forseth. 2018. The Role of Leaf Movements for Optimizing Photosynthesis in Relation to Environmental Variation. In Adams III, W., and Terashima, I. (Eds.), *The Leaf: A Platform for Performing Photosynthesis. Advances in Photosynthesis and Respiration* (pp. 401–423). Springer, Cham. https://doi.org/10.1007/978-3-319-93594-2_14.

Ningthoujam, R., H. Balzter, K. Tansey, K. Morrison, S. Johnson, F. Gerard, C. George, et al. 2016. "Airborne S-Band SAR for Forest Biophysical Retrieval in Temperate Mixed Forests of the UK." *Remote Sensing* 8 (7): 609. https://doi.org/10.3390/rs8070609.

Omar, H., M. Misman, and A. Kassim. 2017. "Synergetic of PALSAR-2 and Sentinel-1A SAR Polarimetry for Retrieving Aboveground Biomass in Dipterocarp Forest of Malaysia." *Applied Sciences* 7 (7). https://doi.org/10.3390/app7070675.

OpenStreetMap. 2017. "Planet Dump." OpenStreetMap Contributors. https://org/Planet.Osm.org .

Pan, L., M. Moghaddam, L. E. Pierce, and R. M. Lucas. 2005. "Radar Backscattering Model for Multilayer Mixed-Species Forests." *IEEE Transactions on Geoscience & Remote Sensing* 43 (11): 2612–2626. https://doi.org/10.1109/tgrs.2005.847909.

Pan, L., L. E. Pierce, and M. Moghaddam. 2005. "Radiative Transfer Model for Microwave Bistatic Scattering from Forest Canopies." *IEEE Transactions on Geoscience & Remote Sensing* 43 (11): 2470–2483. https://doi.org/10.1109/tgrs.2005.853926.

Picard, G., T. Le Toan, S. Quegan, Y. Caraglio, and T. Castel. 2004. "Radiative Transfer Modeling of Cross-Polarized Backscatter from a Pine Forest Using the Discrete Ordinate and Eigenvalue Method." *IEEE Transactions on Geoscience & Remote Sensing* 42 (8): 1720–1730. https://doi.org/10.1109/tgrs.2004.831229.

Pisek, J., A. Erb, L. Korhonen, T. Biermann, A. Carrara, E. Cremonese, M. Cuntz, et al. 2021. "Retrieval and Validation of Forest Background Reflectivity from Daily Moderate Resolution Imaging Spectroradiometer (MODIS) Bidirectional Reflectance Distribution Function (BRDF) Data Across European Forests." *Biogeosciences* 18 (2): 621–635. https://doi.org/10.5194/bg-18-621-2021.

Posada, J. M., R. Sievanen, C. Messier, J. Perttunen, E. Nikinmaa, and M. J. Lechowicz. 2012. "Contributions of Leaf Photosynthetic Capacity, Leaf Angle and Self-Shading to the Maximization of Net Photosynthesis in Acer saccharum: A Modelling Assessment." *Annals of botany* 110 (3): 731–741. https://doi.org/10.1093/aob/mcs106.

Ranson, K. J., G. Sun, J. F. Weishampel, and R. G. Knox. 1997. "Forest Biomass from Combined Ecosystem and Radar Backscatter Modeling." *Remote Sensing of Environment* 59 (1): 118–133. https://doi.org/10.1016/s0034-4257(96)00114-9.

Raymond, W., and S. S. Chaturvedi. 2020. "Relationship Between Above-Ground Biomass and Different Vegetation Indices of Forests of Ri-Bhoi District, Meghalaya, India." *International Journal of Engineering Research And* V9 (5). https://doi.org/10.17577/ijertv9is050128.

Rollinson, C. R., Y. Liu, A. Raiho, D. J. P. Moore, J. McLachlan, D. A. Bishop, A. Dye, et al. 2017. "Emergent Climate and CO 2 Sensitivities of Net Primary Productivity in Ecosystem Models Do Not Agree with Empirical Data in Temperate Forests of Eastern North America." *Global Change Biology* 23 (7): 2755–2767. https://doi.org/10.1111/gcb.13626.

Saatchi, S. S., R. A. Houghton, R. C. Dos Santos AlvalÁ, J. V. Soares, and Y. Yu. 2007. "Distribution of Aboveground Live Biomass in the Amazon Basin." *Global Change Biology* 13 (4): 816–837. https://doi.org/10.1111/j.1365-2486.2007.01323.x.

Saatchi, S. S., and K. C. McDonald. 1997. "Coherent Effects in Microwave Backscattering Models for Forest Canopies." *IEEE Transactions on Geoscience & Remote Sensing* 35 (4): 1032–1044. https://doi.org/10.1109/36.602545.

Sancho-Knapik, D., A. Escudero, S. Mediavilla, C. Scoffoni, J. Zailaa, J. Cavender-Bares, T. G. Alvarez-Arenas, et al. 2021. "Deciduous and Evergreen Oaks Show Contrasting Adaptive Responses in Leaf Mass per Area Across Environments." *The New Phytologist* 230 (2): 521–534. https://doi.org/10.1111/nph.17151.

Santi, E., S. Paloscia, S. Pettinato, G. Fontanelli, M. Mura, C. Zolli, F. Maselli, M. Chiesi, L. Bottai, and G. Chirici. 2017. "The Potential of Multifrequency SAR Images for Estimating Forest Biomass in Mediterranean Areas." *Remote Sensing of Environment* 200:63–73. https://doi.org/10.1016/j.rse.2017.07.038.

Soudani, K., N. Delpierre, D. Berveiller, G. Hmimina, G. Vincent, A. Morfin, and É. Dufrêne. 2021. "Potential of C-Band Synthetic Aperture Radar Sentinel-1 Time-Series for the Monitoring of Phenological Cycles in a Deciduous Forest." *International Journal of Applied Earth Observation and Geoinformation* 104. https://doi.org/10.1016/j.jag.2021.102505.

Stanley, S., V. Antoniou, A. Askquith-Ellis, L. A. Ball, E. S. Bennett, J. R. Blake, D. B. Boorman. 2023. Daily and Sub-Daily Hydrometeorological and Soil Data (2013–2022) [COSMOS-UK]. *NERC EDS Environmental Information Data Centre. (Dataset).* https://doi.org/10.5285/5060cc27-0b5b-471b-86eb-71f96da0c80f.

Stovall, A. E. L., B. Masters, L. Fatoyinbo, and X. Yang. 2021. "TlsleAF: Automatic Leaf Angle Estimates from Single-Scan Terrestrial Laser Scanning." *The New Phytologist* 232 (4): 1876–1892. https://doi.org/10.1111/nph.17548.

Sun, G., D. S. Simonett, and A. H. Strahler. 1991. "A Radar Backscatter Model for Discontinuous Coniferous Forests." *IEEE Transactions on Geoscience & Remote Sensing* 29 (4): 639–650. https://doi.org/10.1109/36.135826.

Takoudjou, M., P. P. Stéphane, B. Sonké, J. Hackenberg, S. Griffon, F. de Coligny, N. Guy Kamdem, et al. 2017. "Using Terrestrial Laser Scanning Data to Estimate Large Tropical Trees Biomass and Calibrate Allometric Models: A Comparison with Traditional Destructive Approach." *Methods in Ecology and Evolution* 9 (4): 905–916. https://doi.org/10.1111/2041-210x.12933.

Terryn, L., K. Calders, M. Disney, N. Origo, Y. Malhi, G. Newnham, P. Raumonen, M. Å Kerblom, and H. Verbeeck. 2020. "Tree Species Classification Using Structural Features Derived from Terrestrial Laser Scanning." ISPRS *Journal of Photogrammetry & Remote Sensing* 168:170–181. https://doi.org/10.1016/j.isprsjprs.2020.08.009.

Treuhaft, R. N., and P. R. Siqueira. 2004. "The Calculated Performance of Forest Structure and Biomass Estimates from Interferometric Radar." *Waves in Random Media* 14 (2): SS345–SS358. https://doi.org/10.1088/0959-7174/14/2/013.

Tsang, L., J. A. Kong, and R. T. Shin. 1984. "Radiative Transfer Theory for Active Remote Sensing of a Layer of Nonspherical Particles." *Radio Science* 19 (2): 629–642. https://doi.org/10.1029/RS019i002p00629.

Ulaby, F. T., and R. P. Jedlicka. 1984. "Microwave Dielectric Properties of Plant Materials." *IEEE Transactions on Geoscience & Remote Sensing* GE-22 (4): 406–415. https://doi.org/10.1109/tgrs.1984.350644.

Ulaby, F. T., K. Sarabandi, K. McDonald, M. Whitt, and M. Craig Dobson. 1990a. "Michigan Microwave Canopy Scattering Model." *International Journal of Remote Sensing* 11 (7): 1223–1253. https://doi.org/10.1080/01431169008955090.

Ulaby, F. T., K. Sarabandi, K. McDonald, M. Whitt, and M. Craig Dobson. 1990b. "Michigan Microwave Canopy Scattering Model (MIMICS) - Version 1.0." https://web.eecs.umich.edu/~lep/mimics.pdf.

Wang, C., W. Zhang, Y. Ji, A. Marino, C. Li, L. Wang, H. Zhao, and M. Wang. 2024. "Estimation of Aboveground Biomass for Different Forest Types Using Data from Sentinel-1, Sentinel-2, ALOS PALSAR-2, and GEDI." *Forests* 15 (1): 215. https://doi.org/10.3390/f15010215.

Wilkes, P., M. Disney, M. B. Vicari, K. Calders, and A. Burt. 2018. "Estimating Urban Above Ground Biomass with Multi-Scale LiDAR." *Carbon Balance and Management* 13 (1): 10. https://doi.org/10.1186/s13021-018-0098-0.

Wismann, V. R., K. Boehnke, and C. Schmullius. 1995. "Monitoring Ecological Dynamics in Africa with the ERS-1 Scatterometer." In *1995 International Geoscience and Remote Sensing Symposium, IGARSS '95. Quantitative Remote Sensing for Science and Applications*, 1523–1525. IEEE: Firenze, Italy.

Woodhouse, I. H., E. T. A. Mitchard, M. Brolly, D. Maniatis, and C. M. Ryan. 2012. "Radar Backscatter is Not a 'Direct measure' of Forest Biomass." *Nature Climate Change* 2 (8): 556–557. https://doi.org/10.1038/nclimate1601.

Xiaodong, H., B. Ziniti, N. Torbick, and M. J. Ducey. 2018. "Assessment of Forest Above Ground Biomass Estimation Using Multi-Temporal C-Band Sentinel-1 and Polarimetric L-Band PALSAR-2 Data." *Remote Sensing* 10 (9): 1424. https://doi.org/10.3390/rs10091424.

Yang, W., H. Kobayashi, X. Chen, K. Nishida Nasahara, R. Suzuki, and A. Kondoh. 2017. "Modeling Three-Dimensional Forest Structures to Drive Canopy Radiative Transfer Simulations of Bidirectional Reflectance Factor." *International Journal of Digital Earth* 11 (10): 981–1000. https://doi.org/10.1080/17538947.2017.1353146.

Yi-Cheng, L., and K. Sarabandi. 1995. "Electromagnetic Scattering Model for a Tree Trunk Above a Tilted Ground Plane." *IEEE Transactions on Geoscience & Remote Sensing* 33 (4): 1063–1070. https://doi.org/10.1109/36.406692.

Zeng, P., W. Zhang, Y. Li, J. Shi, and Z. Wang. 2022. "Forest Total and Component Above-Ground Biomass (AGB) Estimation Through C- and L-Band Polarimetric SAR Data." *Forests* 13:3. https://doi.org/10.3390/f13030442.

Zhen, Z., L. Yang, Y. Ma, Q. Wei, H. Il Jin, and Y. Zhao. 2022. "Upscaling Aboveground Biomass of Larch (Larix Olgensis Henry) Plantations from Field to Satellite Measurements: A Comparison of Individual Tree-Based and Area-Based Approaches." *GIScience & Remote Sensing* 59 (1): 722–743. https://doi.org/10.1080/15481603.2022.2055381.

Zhou, H., G. Zhou, Q. He, L. Zhou, Y. Ji, and X. Lv. 2021. "Capability of Leaf Water Content and Its Threshold Values in Reflection of Soil–Plant Water Status in Maize During Prolonged Drought." *Ecological Indicators* 124:107395. https://doi.org/10.1016/j.ecolind.2021.107395.

Zhu, X., and D. Liu. 2015. "Improving Forest Aboveground Biomass Estimation Using Seasonal Landsat NDVI Time-Series." ISPRS *Journal of Photogrammetry & Remote Sensing* 102:222–231. https://doi.org/10.1016/j.isprsjprs.2014.08.014.